Journal of Solid State Chemistry **153,** 218–230 (2000)
doi:10.1006/jssc.2000.8745, available online at http://www.idealibrary.com on IDEAL®

Single-Crystal Neutron Diffraction Investigations on the Phase Transitions in $CeO_{1.800}$ and $CeO_{1.765}$

E. A. Kümmerle,*,† F. Güthoff,*,† W. Schweika,† and G. Heger*,[1]

*Institute for Crystallography, University of Aachen, Germany; and †Institute for Solid State Research, Research Center Jülich, Germany

Received December 2, 1999; in revised form April 13, 2000; accepted April 20, 2000; published online July 11, 2000

Information on the controversial phase diagram of CeO_y ($1.65 < y \leq 2.0$) was obtained by making single-crystal neutron scattering measurements on $CeO_{1.800}$ and $CeO_{1.765}$ up to 1064 K. The observed phase transitions at 755 K, 823 K, 866 K, and 898 K when the temperature is raised (or 738 K, 773 K, 845 K, and 898 K when T is lowered) for $CeO_{1.800}$ as well as the observed phase transition at 911 K (907 K) for $CeO_{1.765}$ qualitatively confirm the phase diagram proposed previously by Ricken *et al.* The crystal structures of all the observed phases apparently are of rhombohedral symmetry (space group $R\bar{3}$).

INTRODUCTION

The phase diagram of CeO_y is still not known very well. There are many discrepancies between the results of different authors, especially for the composition range $1.75 < y < 1.85$. Extensive specific heat measurements in that composition range by Ricken *et al.* (1) yielded a phase diagram that differs tremendously from the phase diagram published by ASM International (2). The aim of the present work was to decide in favor of one of the contradictory diagrams using single-crystal neutron scattering as a completely different method to detect the various phases. Furthermore, some information on the crystal structures of these phases was intended to be obtained. Due to the experimental difficulties in varying the oxygen content of a single crystalline sample, the measurements were taken for two constant compositions $y = 1.800$ and $y = 1.765$.

SAMPLE PREPARATION

The single-crystal specimen with a volume of approximately 1 cm^3 used for these neutron diffraction measurements was a piece of a large unique single crystal. Other parts of that crystal were used for the neutron diffraction structure investigations on C–$Ce_2O_{3+\delta}$, Ce_7O_{12}, and $Ce_{11}O_{20}$ described elsewhere (3, 4).

The crystal of about 2 cm^3 was grown by skull melting at the Institute of Physics of the University of Frankfurt, Germany, using CeO_2 with a purity of 99.9%. Its color was pale pink.

The structure refinement of a piece of that CeO_2 single crystal by neutron diffraction proved its fluorite-type cubic structure (space group $Fm\bar{3}m$) with a full occupation of the oxygen site (sof = 101(1)%). The mean square displacements were determined to be $U(\mathrm{Ce}) = 0.0036(2)\,\text{Å}^2$ and $U(\mathrm{O}) = 0.0064(2)\,\text{Å}^2$ (3, 4).

To reduce the specimen to the composition $CeO_{1.800}$ it was heated for about 20 h in a well-defined humidified hydrogen (purity 5.0) atmosphere at 971°C using the relationship between the composition y of CeO_y and the oxygen pressure according to Bevan and Kordis (5). After the reduction it was tempered in argon (original purity 4.8, cleaned by Oxisorb and porous zirconium at 800°C (1)) which caused a certain reoxidation (see Table 2.1 in (4) or compare Table (1) in this article and Table 1 in (3)). Then the crystal was sealed in a niobium container to prevent it from reoxidizing.

After the completion of the investigations on $CeO_{1.800}$ the specimen was reduced in the same way to the composition $CeO_{1.765}$ without tempering it afterwards. Due to the embrittlement caused by the reduction some parts of the crystal crumbled away, leaving a remaining specimen of about 0.5 cm^3.

The reduction conditions for both compositions are summarized in Table 1. The specimen was black for both reduction levels. The final compositions were determined from measurements of the pseudocubic lattice parameter a by neutron diffraction using the well-known relationship between the composition y and a (6). a was determined with an accuracy of ± 0.002 Å, and the accuracy of y is about ± 0.004 (neglecting the error in the relationship between y and a that is not specified in (6)).

[1] To whom correspondence should be addressed. Fax: + 49 241 8888184. E-mail: heger@kristall.xtal.rwth-aachen.de.

0022-4596/00 $35.00

TABLE 1

Reduction Conditions and Final Compositions *y* Determined from Measurements of the Pseudocubic Lattice Parameter *a* Using the Relationship between *y* and *a* According to Ray *et al.* (6)

y	*a* (Å)	Reduction conditions
1.800	5.502	$T = 971°C$, $T_B = 3°C$, tempered for 16 h at 1000°C, initial composition: CeO_2
1.765	5.517	$T = 971°C$, $T_B = 3°C$, mixed 1:5.5 with dry H_2, initial composition: $CeO_{1.800}$

Note. The errors are ± 0.002 Å for *a* and ± 0.004 for *y*. *T* is the reduction temperature, and T_B is the water temperature in the hydrogen humidifier.

NEUTRON DIFFRACTION MEASUREMENTS

For a rough overall view on the diffraction, intensity maps of the elastic neutron scattering intensity in the $(1\,\bar{1}\,0)$ plane and in the layer 0.25 of the $[1\,\bar{1}\,0]$ zone, i.e., in a plane in the reciprocal space parallel to $[1\,\bar{1}\,0]$ with the distance $0.25 \cdot [1\,\bar{1}\,0]$ to that (the $(1\,\bar{1}\,0)$ itself is the layer 0), were collected at the time-of-flight spectrometer for diffuse neutron scattering (DNS) at the FRJ-2 research reactor (DIDO) in the Research Center Jülich, Germany. This facility uses cold neutrons (moderated with liquid hydrogen). A double-focusing graphite monochromator was used to select a neutron wavelength of 3.3 Å. Pure elastic scattering was achieved by the time-of-flight method with an energy resolution of ± 1.5 meV. Fifty-two ^{3}He detectors were arranged in such a way that the scattered intensity in the 2θ range from 0 to 128° could be measured simultaneously for one sample orientation ϕ with a resolution of $\Delta(2\theta) = 2.5°$. The sample was then reoriented in steps of $\Delta\phi = 1°$. The sample container caused an intense Debye–Scherrer ring (Nb 1 1 1 reflection) in the diffraction measurements. Because of the vertical divergence the integration widths of the layers are 0.15 reciprocal lattice units (i.e., $\pm 0.15 \cdot [1\,\bar{1}\,0]$) for the layer 0 and ± 0.1 for the layer 0.25.

To investigate in detail the structural phase transitions which occur between the phases with different ordering of oxygen vacancies, measurements of the elastic neutron scattering intensity in the $(1\,\bar{1}\,0)$ plane were taken using the triple-axis spectrometer UNIDAS at the FRJ-2 research reactor (DIDO) in the Research Center Jülich, Germany. A vertically focusing graphite double monochromator was used to select 2.36 Å neutrons from the thermal neutron source. The scattered neutron wavelength was selected using a focusing graphite analyzer. The neutron beam divergence was controlled by Rutherford collimators (collimation parameters $(\alpha_2, \alpha_3, \alpha_4, \alpha_5) = (24', 15', 15', 15')$), the neutron detection was done using ^{3}He detectors. The measurements were concentrated on the 2 2 0 and 0 0 4 reflections of the fluorite structure and on selected superstructure reflections. The sample was heated in a standard oven of UNIDAS; the temperature was measured with two thermocouples fixed in the sample holder at about 1 cm above and below the sample.

$CeO_{1.800}$

The maps taken at the DNS at ambient temperature are shown in Fig. 1. A great number of superstructure reflections in both layers are in accordance with cubic symmetry. Especially in the ranges $\xi\xi\zeta$ of the $(1\,\bar{1}\,0)$ plane with $\xi = 1.6 \pm 0.3$, $|\zeta| = 1.0 \pm 0.4$ and $\xi = 1.3 \pm 0.2$, $|\zeta| = 1.6 \pm 0.2$, these reflections are very intense and close together. In the range $\xi = 1.6 \pm 0.3$, $|\zeta| = 1.0 \pm 0.4$ the superstructure reflections lie on the straight lines $[\xi\xi\xi/2]$ and $[\xi\xi 2\text{-}\xi/2]$ within the experimental accuracy given here. In the layer 0.25 the most intense superstructure reflections are located in the range $\xi + 0.25\ \xi - 0.25\ \zeta$ with $\xi = 1.45 \pm 0.1$, $0.2 < |\zeta| < 2.0$ and again, their positions are in accordance with cubic symmetry.

Apart from these reflections, there is a ring of arbitrarily distributed reflections with the radius of the 2 2 0 reflection of CeO_2 which originate from small misoriented parts of the crystal. (The 2 2 0 reflection of CeO_2 is much more intense than the 2 0 0 and the 1 1 1 reflections, so only the ring of the 2 2 0 reflections is visible.) The arched, extended intensities in the ranges $\xi\xi\zeta$ with $0.8 < \xi < 2.1$, $0 \le |\zeta| < 0.9$ and $\xi = 0.3 \pm 0.1$, $1.1 \le |\zeta| < 3$ in the $(1\,\bar{1}\,0)$ plane and in the corresponding regions in the layer 0.25 as well as the lines crossing in the points $\xi = 0$, $|\zeta| = 1.8$ are caused by multiple reflections in which the niobium container or parts of the heating facility are involved; i.e., these patterns are experimental artifacts.

A map of the $(1\,\bar{1}\,0)$ plane taken at 700 K (not shown here) does not differ significantly from that taken at ambient temperature. The map taken at 850 K (see Fig. (2)) shows that some of the superstructure reflections have already vanished while others are still present. Additionally, a weak diffuse scattering pattern occurs with maxima at $\xi\xi\zeta$, $\xi = 1.56$, $\zeta = 1.07$ and at $\xi = 1.32$, $\zeta = 1.66$. At 1000 K all the superstructure reflections have vanished and the intensity of the diffuse scattering is much increased. This high-temperature diffuse scattering and its information concerning the oxygen vacancy short-range order in the disordered phase are discussed elsewhere (4).

At the UNIDAS the superstructure reflections near the straight lines $[\xi\xi\xi/2]$ and $[\xi\xi 2\text{-}\xi/2]$ with $1.3 < \xi < 2.0$ were selected for detailed temperature-dependent investigations. Figure 3 shows a high-resolution measurement of the diffraction intensity map of that area in the $(1\,\bar{1}\,0)$ plane taken at 667 K, i.e., in the low-temperature phase. The raster stepwiths of the measurements are $\delta\xi = 0.004$ and $\delta\Delta l = 0.01$

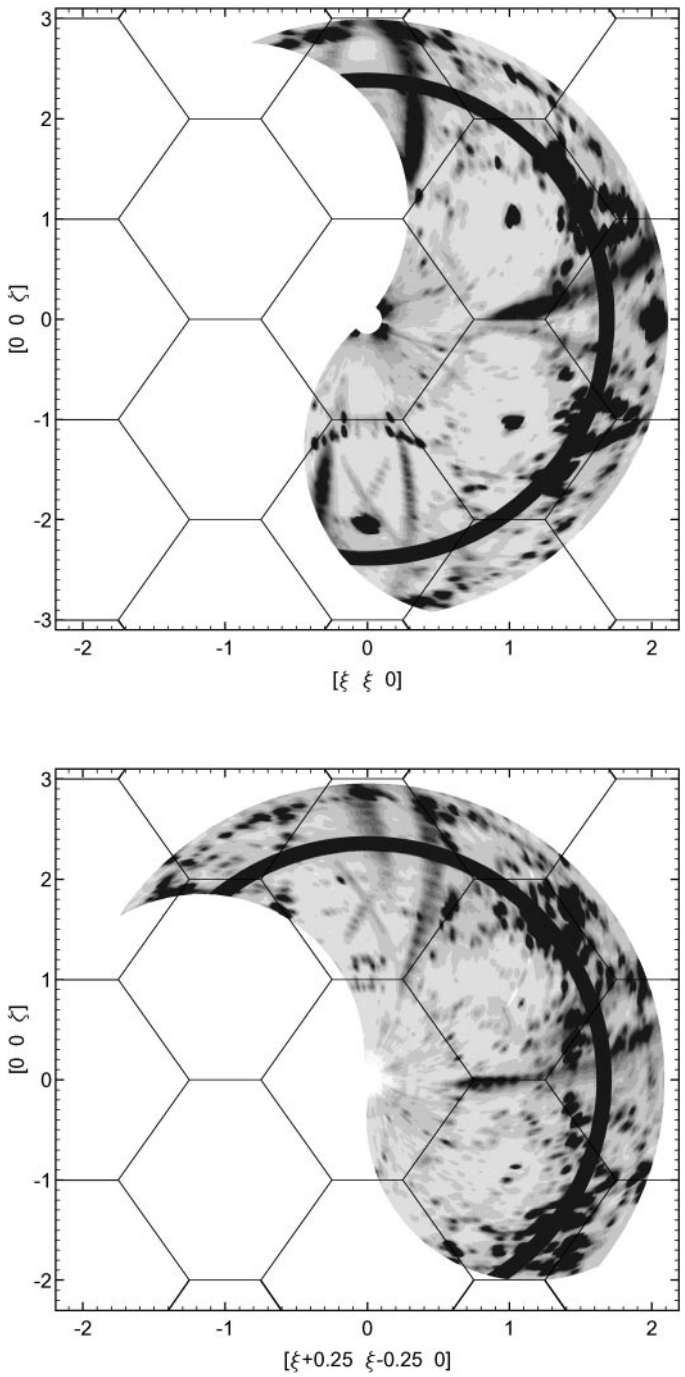

FIG. 1. Figure Contour plots of the elastic scattering intensity of $CeO_{1.800}$ at ambient temperature in the layer 0 (top) and in the layer 0.25 (bottom) of the $[1\,\bar{1}\,0]$ zone. The arched, extended intensity patterns are multiple reflections caused by the experimental environment (see the text).

for $-0.05 \leq \Delta l \leq 0.02$ or $\delta\Delta l = 0.02$ for $0.02 \leq \Delta l \leq 0.06$, respectively.

The elliptic shapes of the reflections show the different reflection widths in the longitudinal or transversal direc-

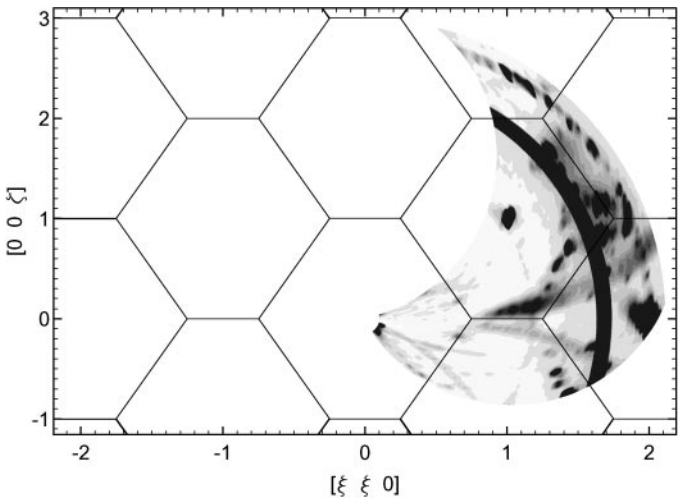

FIG. 2. Contour plot of the elastic scattering intensity of $CeO_{1.800}$ at 850 K in the layer 0. (Again, the arched intensity patterns are caused by the experimental environment.)

tions (FWHM $= 0.017\,\text{Å}^{-1}$ longitudinal and $1.3^\circ \approx 0.06\,\text{Å}^{-1}$ transversal). The centers of the reflections in the top and in the bottom part of the figure are located mirror symmetrical with respect to the plane $l = 1$ (it is a line in the figure projection), but their intensities are different. The reflections at the positions $\xi = 1.473$, 1.640, 1.756, and 1.84 are located rather precisely on the straight lines $[\xi\xi\xi/2]$ or $[\xi\xi 2\text{-}\xi/2]$, in contrast to the reflections at $(\xi, \Delta l) = (1.485, -0.03)$, $(1.64, -0.04)$, and $(1.793, -0.02)$ in the $\xi\xi\xi/2 + \Delta l$ array and at the corresponding positions in the $\xi\xi 2\text{-}\xi/2 + \Delta l$ array. In these experiments it was not possible to determine whether the reflection positions lie significantly outside of the $(1\,\bar{1}\,0)$ plane.

The sharpness of the reflections undoubtedly shows that there is a superstructure on the fluorite lattice and not merely short-range order. The reflection positions show that the supercell (or supercells in the case of coexisting phases in the sample) must be of large periodicity because there is no way to find indices h/n, k/n, l/n for the reflections choosing small numbers for n.

Temperature dependence of the superstructure reflections. To determine the number of phase transitions and the transition temperatures the superstructure reflections at $\xi\xi\xi/2$ and $\xi\xi 2\text{-}\xi/2$, $1.3 < \xi < 2.0$, were observed at different temperatures, both when raising and when lowering the temperature. To get a rough overview, the sample was heated in large steps of 50 K, scanning the above-mentioned reflections at each temperature level. The measurements showed that the phase transitions occur between 750 K and 950 K and indicate which positions in the **Q** space are of interest. That temperature range was then remeasured by raising the temperature in steps of 10 K and scanning only

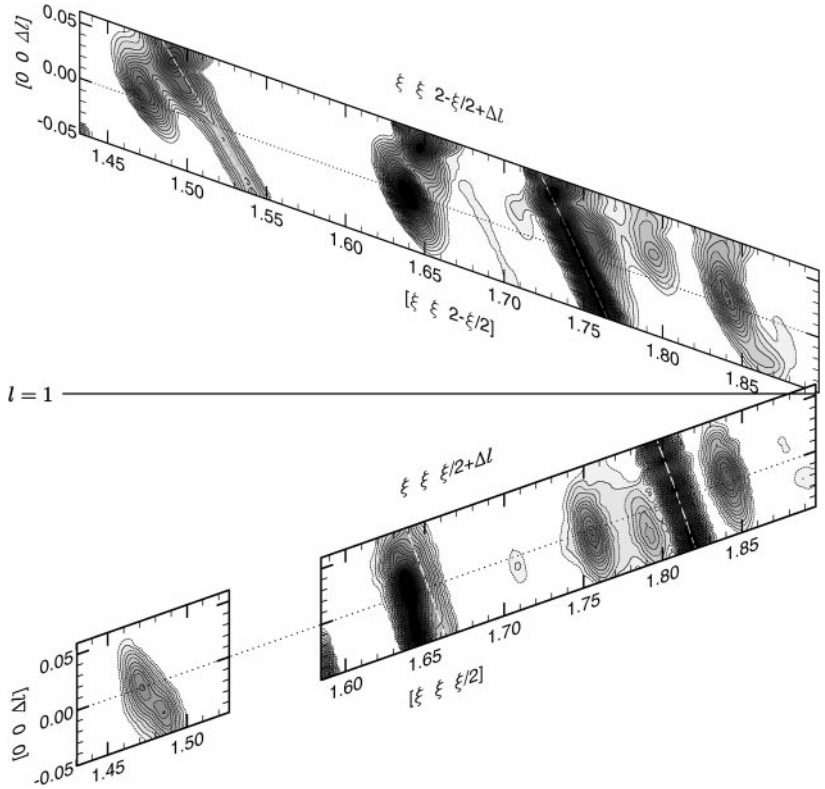

FIG. 3. Contour plot of the elastic scattering intensity of $CeO_{1.800}$, low-temperature phase (667 K), in the $(1\,\bar{1}\,0)$ plane in the areas $\xi\xi\xi/2 + \Delta l$ and $\xi\xi 2\text{-}\xi/2 + \Delta l$. The dashed white lines show the positions of the Debye–Scherrer rings of Mo 1 1 1 and Al 2 0 0 (heating facility components). A small part of the Nb 1 1 1 ring can be seen in the bottom part of the figure at $\xi \approx 1.58$.

the interesting **Q** regions. Each temperature level was kept for about 75 minutes while the scattering data were taken. Figure 4 shows that the reflection pattern changes drastically as a function of temperature. In the whole observed **Q** range the changes occur simultaneously at definite temperatures within a relatively small temperature range. Consequently, the phase transition temperatures can be determined easily with an absolute precision of about ± 5 K (relative precision ± 1 K). There are four phase transitions at 755 K, 823 K, 866 K, and 898 K, labeled in the following T1, … ,T4. The ranges between them are labeled R1, … ,R5 (R1, $T < 755$ K; … ;R5, $T > 898$ K).

In the range R4, i.e., between 866 K and 898 K, the intensities of the two reflections at $\xi\xi\xi/2$ and $\xi\xi 2\text{-}\xi/2$ with $\xi = 1.84$ decrease almost continuously until they have vanished at 898 K. But even these two phase transitions at 866 K and 898 K are clearly visible, particularly when looking at the reflections $\xi\xi\xi/2$, $\xi = 1.635$, and $\xi\xi 2\text{-}\xi/2$, $\xi = 1.425$ and $\xi = 1.617$. It is remarkable that above 823 K the mirror symmetry of the reflection positions with respect to the plane $l = 1$ disappears.

In order to study any hysteresis effects the same **Q** regions were scanned while lowering the temperature in steps of 5 K. Again, each temperature level was kept for about 75 minutes while taking the scans shown in Fig. 4 (right part). Here too, four phase transitions are clearly visible with the reflection patterns in the five ranges matching the corresponding patterns observed before when raising the temperature. So it can be assumed that in both cases the same phases are present.

As shown in Table (2), some phase transition temperatures depend considerably on whether the temperature was raised or lowered. In view of the slow temperature changes (the mean temperature change rates were $+8$ K/h and -4 K/h) together with the temperature measurement very close to the sample, it can be ruled out that these observations are caused by a delayed alignment of the sample temperature. The phase transitions T1, T2, and T3 show real hysteresis effects as they are a common feature of reconstructive phase transitions.

The continuous intensity change of the reflections at $\xi\xi\xi/2$ and $\xi\xi 2\text{-}\xi/2$ with $\xi = 1.84$ within the range R4 observed when raising the temperature is far weaker when lowering the temperature. Here, the changes are concentrated much more at the phase transitions. Instead, the reflections $\xi\xi\xi/2$, $\xi = 1.84$, and $\xi\xi 2\text{-}\xi/2$, $\xi = 1.84$ belonging to range R3 are smeared out into the range R2.

In summary, these measurements show that up to a temperature of about 898 K superstructure reflections are

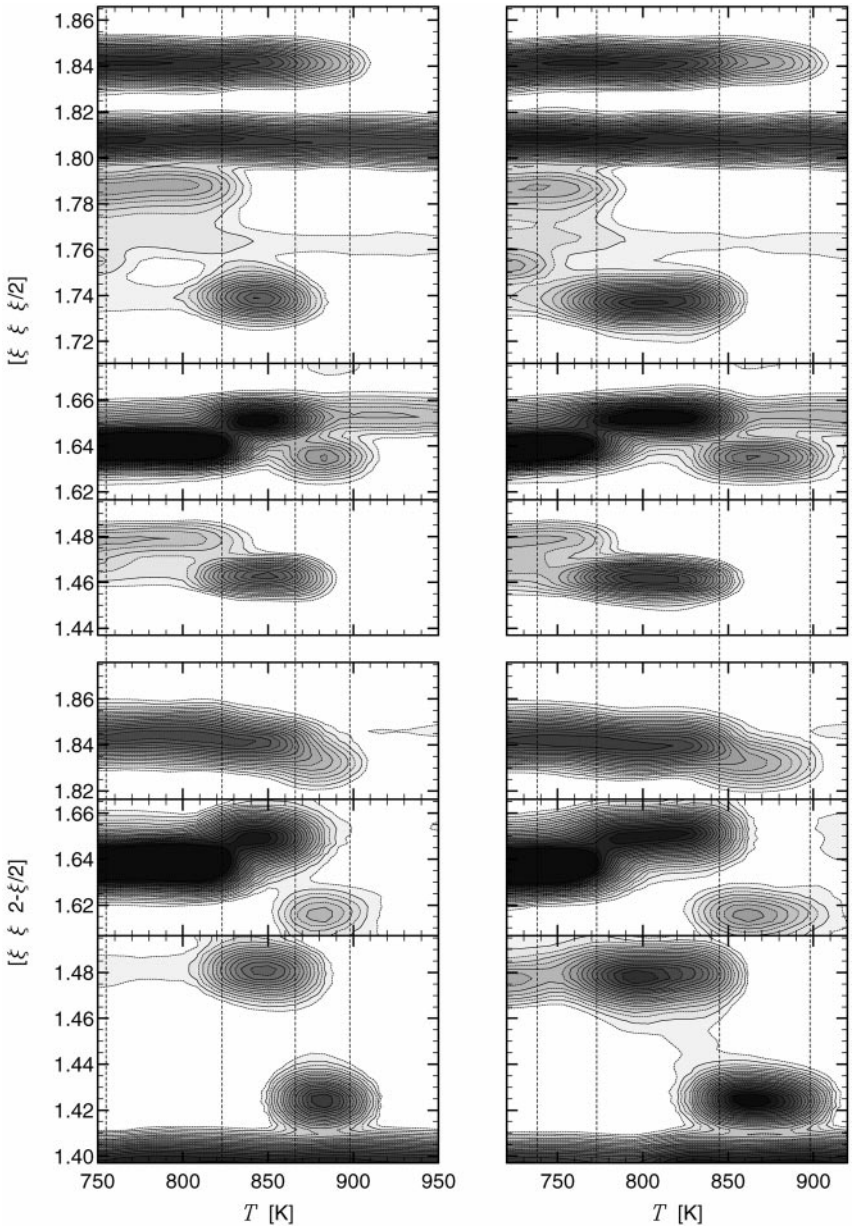

FIG. 4. Contour plots of the [ξξξ/2] (top) and [ξξ2-ξ/2] (bottom) scans for $CeO_{1.800}$ when the sample temperature is raised (left) or lowered (right). At $\xi = 1.653$ and 1.807 in the upper parts of the figure are the Debye–Scherrer rings of Mo 1 1 1 and Al 2 0 0. At the lower border of the lower parts of the figure the Debye–Scherrer ring of Nb 1 1 1 can be seen. The dashed lines show the temperatures of the observed phase transitions.

present and therefore we conclude that the oxygen vacancy arrangement shows a periodic ordering. However, already at 850 K, there is a diffuse scattering component (see Fig. 2) indicating partial disorder in the vacancy structure. At each of the phase transitions T1–T4 the vacancy order does change as proved by the obvious change in the reflection pattern. But all these superstructures must have some characteristic features in common, as shown by the strong superstructure reflections located in the same **Q** space regions for all these phases; see the measurements presented in that paragraph and the DNS measurements presented at the beginning of the section.

Temperature dependence of the fluorite structure reflections. To determine the splitting of the fluorite structure reflections transversal and longitudinal scans of selected reflections were taken at different temperatures.

There is no difference between the longitudinal profiles of the 0 0 4 reflection in the low-temperature range R1 and the high-temperature range R5. The widths of both profiles

TABLE 2

Comparison of the Phase Transition Temperatures $T^{\uparrow}$ and $T^{\downarrow}$ Observed for $CeO_{1.800}$ When the Temperature Is Raised or Lowered, Respectively ($\bar{T} = (T^{\uparrow}+T^{\downarrow})/2$, $\Delta T = T^{\uparrow}-T^{\downarrow}$)

Transition	$T^{\uparrow}$	$T^{\downarrow}$	$\bar{T}$	ΔT
T1	755	738	746	17
T2	823	773	798	50
T3	866	845	855	21
T4	898	898	898	0

($0.026\,\text{Å}^{-1}$ at 667 K, $0.025\,\text{Å}^{-1}$ at 987 K) do not differ significantly and correspond to the longitudinal resolution of the UNIDAS; both profiles can be fitted with single Gaussian functions. So there is no indication of any reflection splitting. These two profiles were used to determine the pseudocubic lattice parameter $a(295\,\text{K}) = 5.502(2)\,\text{Å}$ (extrapolated to ambient temperature) and the thermal linear expansion coefficient $1.3(1)\times10^{-5}\,\text{K}^{-1}$, in good agreement with values for CeO_2 (7–9).

The integral intensity of the 0 0 4 reflection is almost equal for both temperatures. The intensity loss at high temperature according to the Debye–Waller factor seems to be compensated by the intensity gain due to the vanishing of the superstructure reflections.

The results for the longitudinal 2 2 0 reflection profiles are quite different, see Fig. 5. In the ranges R1–R4 that reflection is split; only in the high-temperature range R5 can its profile be fitted with a single Gaussian function. For the ranges R1–R3 the profiles can be fitted using the sum of two Gaussian components, see Table 3, yielding FWHM values for these components that are in accordance with the longitudinal resolution of the UNIDAS. Trying the same for the range R4 the resulting reflection widths were significantly too large, so a third component was used. But due to the highly correlated fit parameters the precise positions and especially the partial intensities of the individual components could not be determined precisely for that profile. The components shown in Fig. 5 and listed in Table 3 are determined applying the constraint of equal width parameters for the three Gaussian functions.

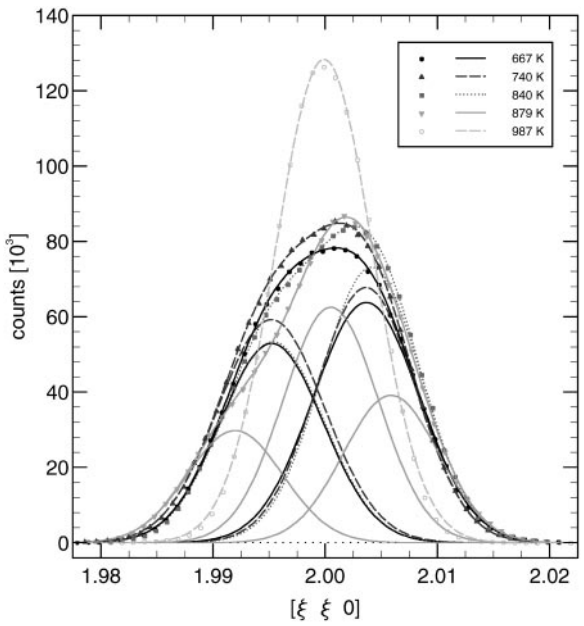

FIG. 5. Longitudinal scans of the 2 2 0 fluorite structure reflection for $CeO_{1.800}$ at 667 K (range R1), 740 K (R2), 840 K (R3), 879 K (R4), and 987 K (R5). For each profile the Gaussian components and the sum function (cf. Table 3) are plotted.

Finally, Fig. 6 shows transversal (rocking) profiles of the 2 2 0 and the 0 0 4 reflections. The widths of the two profiles are almost equal, FWHM = 1.2°. The comparison with the spectrometer resolution of about 0.15° for the used configuration shows that the observed profile widths must be due to the mosaicity of the sample crystal. Because of that, reflection splitting cannot be observed in any transversal scan.

$CeO_{1.765}$

The maps taken at the DNS at ambient temperature are shown in Fig. 7. For $CeO_{1.765}$ too, a great number of superstructure reflections can be seen in the two layers, but now, the cubic symmetry is obviously violated. (As for $CeO_{1.800}$, there are rings of reflections due to misoriented parts of the crystal and multiple reflections caused by the experimental environment.)

Additionally to the Brillouin zones of the fluorite structure the zones of a seven-fold superstructure are drawn in Fig. 7 showing that in the layer 0 many of the superstructure reflections are located on positions that are shifted by $\Delta\xi = \frac{1}{7}$ off the superstructure zone center positions and in the layer 0.25 many reflections lie at the zone centers. Comparison with the reflection positions for the Ce_7O_{12} structure (3, 4) further shows that almost all of these reflections can be identified with Ce_7O_{12} reflections. That part of the reflections observed in the layer 0 can be identified with Ce_7O_{12} reflections being located in the layer $\frac{1}{7} \approx 0.143$ (that explains the shift of $\Delta\xi = \frac{1}{4}$) and that part observed in the layer 0.25 can be identified with Ce_7O_{12} reflections being located in the layer $\frac{2}{7} \approx 0.286$, in accordance with the abovementioned thicknesses of the measured layers.

Since the reflections belonging to (noncubic) Ce_7O_{12} do not show pseudocubic symmetry, we conclude that the volume fractions of the eight possible orientation domains are not equal.

Additionally, there are some reflections that are not compatible with a seven-fold superstructure. In the layer 0, most of them are located in the ranges $\xi\xi\zeta$, $\xi = 1.6 \pm 0.2$, $|\zeta| = 1.0 \pm 0.2$. Moreover, there are some reflections that seem to

TABLE 3
Parameters of the Profile Fits for the Longitudinal Scans of the 2 2 0 Reflection for $CeO_{1.800}$ Using the Function $\sum_i A_i \exp(-(\xi - B_i)^2/2\sigma_i^2)$

Range	T (K)	I	S	i	$A_i(10^3)$	B_i	σ_i	w_i (Å^{-1})
R1	667	1361	1.9999	1	53(2)	1.9952(2)	0.00458(7)	0.0173(3)
				2	64(2)	2.0037(2)	0.00471(6)	0.0178(3)
R2	740	1456	1.9996	1	59(2)	1.9952(2)	0.00474(8)	0.0179(3)
				2	68(2)	2.0036(2)	0.00444(6)	0.0168(3)
R3	840	1425	2.0004	1	53(2)	1.9953(2)	0.00456(9)	0.0172(4)
				2	73(2)	2.0041(1)	0.00445(6)	0.0168(3)
R4	879	1399	2.0002	1	30(1)	1.9920(1)	0.00425(6)	0.0161(3)
				2	62(2)	2.0005(2)	0.00425(6)	0.0161(3)
				3	39(2)	2.0059(2)	0.00425(6)	0.0161(3)
R5	987	1392	1.9999	1	128(1)	1.9999(0)	0.00433(2)	0.0163(1)

Note. The FWHM values of the Gaussian components are $w_i = \sigma_i\sqrt{8\ln 2}\sqrt{2}(2\pi/a)$. I is the integral and S the center of gravity of the fit function.

be compatible with a seven-fold superstructure but are incompatible with the reflection positions of Ce_7O_{12}, for example the reflection $(\xi,\zeta) \approx (10/7, 5/7)$. So, apart from the phase Ce_7O_{12}, at most one more phase is present in the sample crystal.

A map of the $(1\,\bar{1}\,0)$ plane taken at 850 K (not shown here) differs only a little from that taken at ambient temperature. In contrast to the map for $CeO_{1.800}$ at 850 K, no diffuse scattering intensity was observed.

Again, selected superstructure and fluorite structure reflections were measured at the UNIDAS now. Here too, the Ce_7O_{12} reflections from the layer $\frac{1}{7}$ appear in the $(1\,\bar{1}\,0)$ plane due to the vertical divergence of the spectrometer.

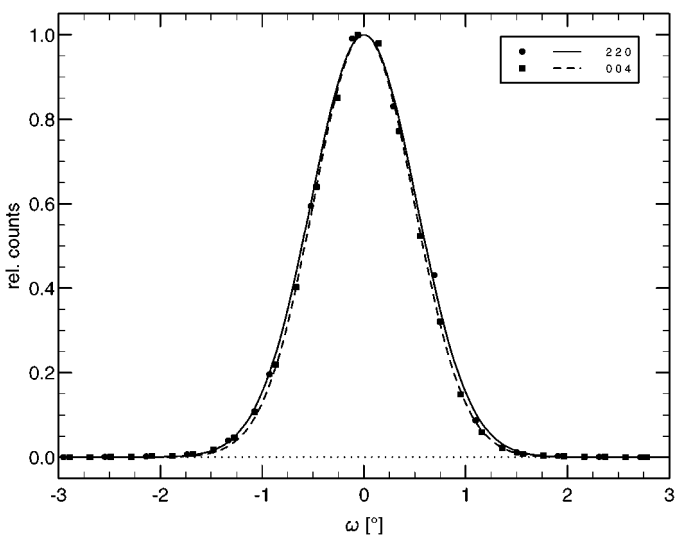

FIG. 6. Transversal scans of the 2 2 0 and the 0 0 4 reflections for $CeO_{1.800}$ at 667 K.

Temperature dependence of the reflections. To get a rough overview of the phase transitions, the sample was heated in large steps of 40 K starting at 600 K. Longitudinal scans of the fluorite structure reflections 0 0 4 and 2 2 0 and scans in the direction $\xi\xi 0$ of the superstructure reflections $\xi\xi\zeta$ with $(\xi,\zeta) \approx (1.56, 1.143) \approx (11/7, 8/7)$, that is the $\bar{1}\,3\,0_r$ reflection of Ce_7O_{12} (rhombohedral setting) which is shifted a little due to the rhombohedral distortion of the Ce_7O_{12} lattice, and $(\xi,\zeta) \approx (1.64, 1.143)$ which does not belong to Ce_7O_{12} were taken. Between 880 K and 920 K the profiles of the fluorite structure reflections changed and the superstructure reflection not belonging to Ce_7O_{12} vanished.

The temperature range around 900 K was then remeasured while the temperature was raised as well as lowered in steps of 5 K by scanning the same reflections as before. When the temperature was raised, the fluorite structure reflection 1 1 1 and the superstructure reflection at $(\xi,\zeta) \approx (1.43, 0.714)$ not belonging to Ce_7O_{12} were scanned additionally. While taking the scattering data, each temperature level was kept for about 130 minutes (when raising the temperature) or 90 minutes (when lowering the temperature), respectively. The results are shown in Fig. 8.

The changes in the three fluorite structure reflection profiles and the vanishing of the superstructure reflection not belonging to Ce_7O_{12} obviously occur at the same temperature, so there exists one single phase transition. The transition temperature is 911 K when raising and 907 K when lowering the temperature (with an absolute precision of about $\pm$ 5 K and a relative precision of about $\pm$ 1 K); i.e., there is a hysteresis of about 4 K. The ranges below and above the transition are labeled in the following with R1 and R2, respectively.

The superstructure reflection belonging to Ce_7O_{12} does not change at that phase transition. The transition from Ce_7O_{12} to the disordered high-temperature phase could not

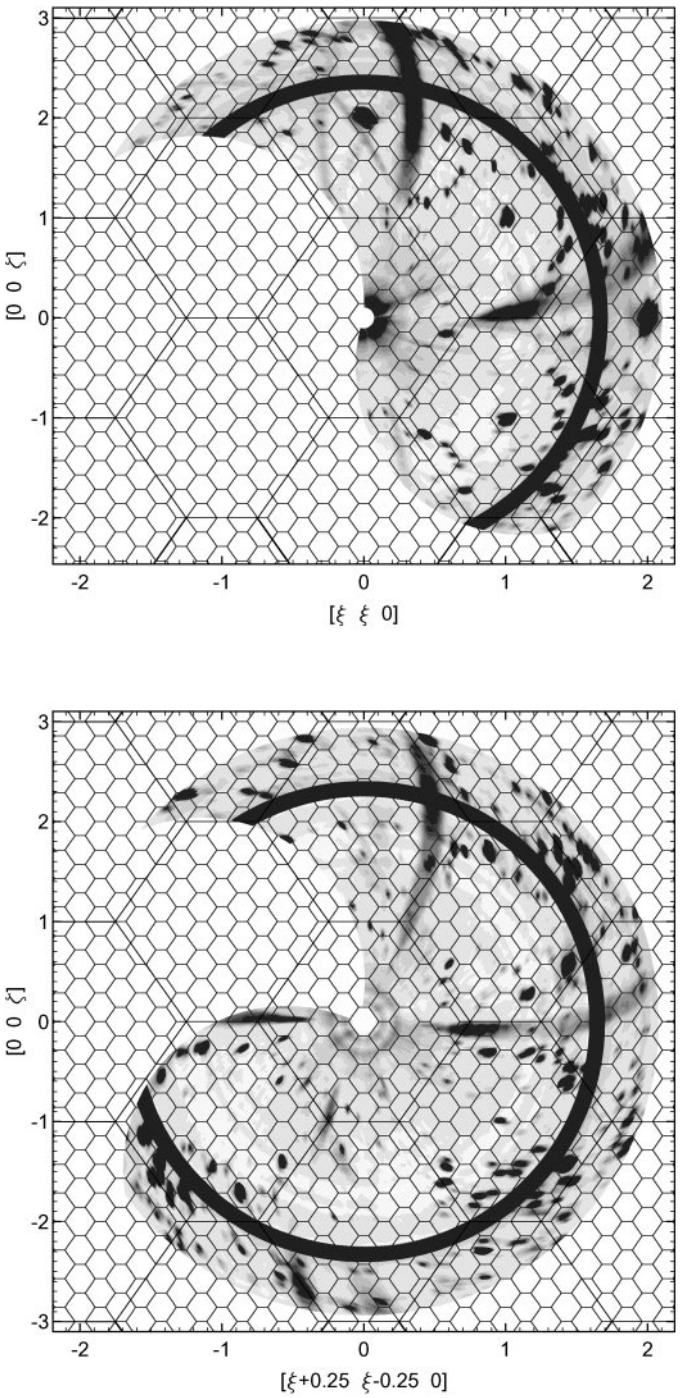

FIG. 7. Contour plots of the elastic scattering intensity of $CeO_{1.765}$ at ambient temperature in the layer 0 (top) and in the layer 0.25 of the $[1\,\bar{1}\,0]$ zone (bottom). In addition to the Brillouin zones of the fluorite structure the zones of a seven-fold superstructure are shown. (Here, too, the arched intensity patterns are caused by the experimental environment.)

be observed up to the maximum temperature of 1064 K that could be reached in the heating facility. This phase transition was investigated in another experiment (3, 4) and found at 1072 K when the temperature was raised and at 1065 K when it was lowered.

At the phase transition observed here, the profiles of the fluorite structure reflections change drastically, see the Figs. 9–11.

Below the phase transition, the 0 0 4 reflection is clearly split into two components, but also above it, two components are necessary to describe the reflection profile (Fig. 9). Using only one component yields FWHM values that are significantly too large. Moreover, for 923 K the reflection profile is clearly asymmetrical. Above the phase transition, the distance between the centers of gravity of the two components decreases when raising the temperature. The two profiles below the phase transition (at 598 K and 895 K) differ considerably, too. An analysis of the reflection profiles

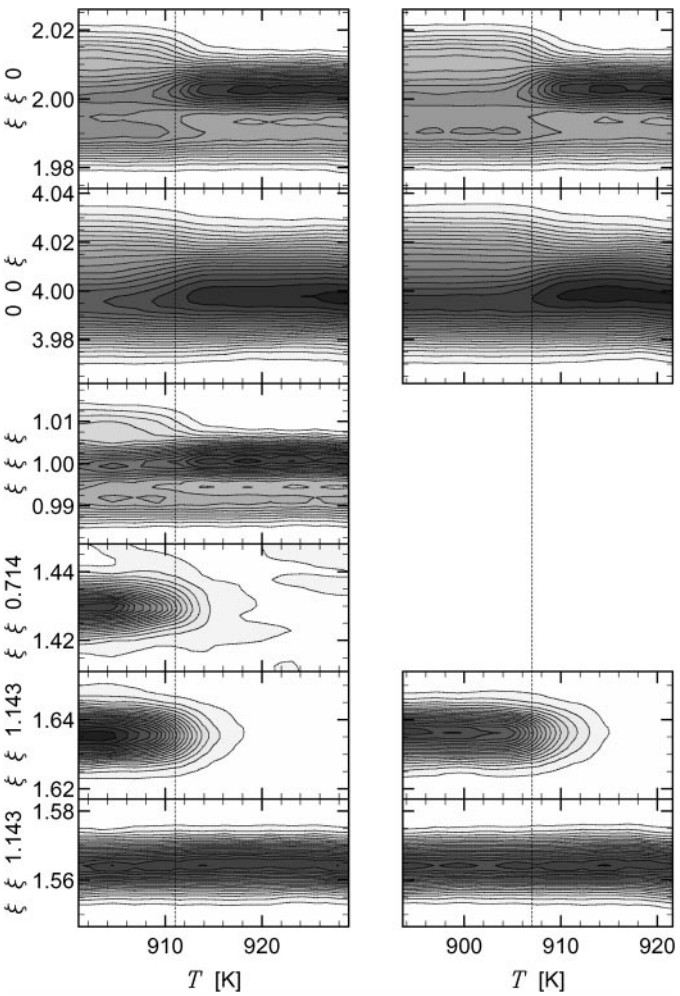

FIG. 8. Contour plots of the intensity profiles for the fluorite structure reflections 2 2 0, 0 0 4, and 1 1 1 and for the superstructure reflections at $\xi\xi\xi$, $(\xi, \zeta) \approx (1.56, 1.143)$, $(1.64, 1.143)$, and $(1.43, 0.714)$ of $CeO_{1.765}$ when the sample temperature is raised (left) or lowered (right). The dashed line shows the temperature of the observed phase transition.

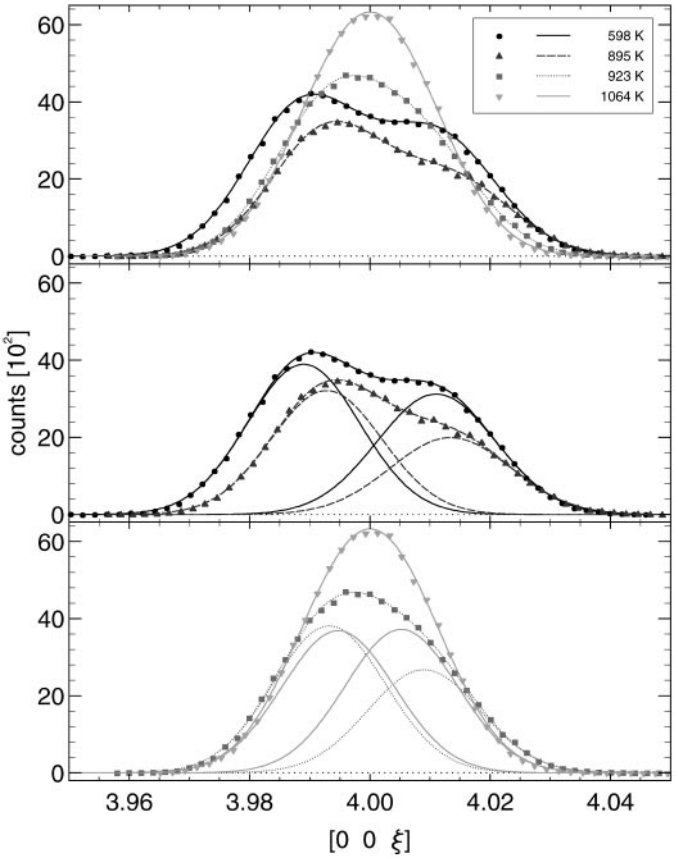

FIG. 9. Longitudinal scans of the 0 0 4 fluorite structure reflection of $CeO_{1.765}$ at 598 K, 895 K, 923 K, and 1064 K. (Top) Comparison of the fit functions for all four temperatures. Each function consists of two Gaussian components. (Middle) For each profile taken below the phase transition (598 K and 895 K) the two Gaussian components and the sum function are plotted. (Bottom) The same for the profiles taken above the phase transition (923 K and 1064 K). (Cf. Table 4.)

at temperatures in between showed that this change occurs continuously.

The fit parameters for the 0 0 4 reflection profiles at the different temperatures are listed in Table 4. The yielded FWHM values for the Gaussian components correspond to the longitudinal resolution of the UNIDAS. The fit for the data taken at 923 K was done with the constraint $\sigma_1 = \sigma_2$. For the data taken at 1064 K the values of σ_1 and σ_2 were fixed at the value determined for 923 K.

The scans of the 0 0 4 reflection were also used to determine the pseudocubic lattice parameter $a(295\,\mathrm{K}) = 5.517(2)$ Å. Due to the complicated reflection profile and its temperature dependence the expansion coefficient could not be determined precisely, so the value $1.3(1) \times 10^{-5}\,\mathrm{K}^{-1}$ determined for $CeO_{1.800}$ was used.

The 2 2 0 reflection is split into four components below the phase transition and into three components above it, as shown in Fig. 10. At first glance, only three components below and two components above the transition are visible, but when the profiles were fit with only three or two Gaussian components, respectively, the FWHM values for the components were significantly too large and not at all uniform. Adding one more component results in FWHM values for all components matching the resolution of the UNIDAS; see the fit parameters listed in Table 4. For all the fits the constraint $\sigma_1 = \sigma_2 = \sigma_3\ (= \sigma_4)$ was applied and for the 1064 K fit the value of σ_i $(i = 1, \ldots, 4)$ was fixed at the value determined for 923 K. For the 2 2 0 reflection too, a continuous profile change was observed below the phase transition.

Figure 11 shows two scans of the 1 1 1 reflection, one below and one above the phase transition. The profile below the transition obviously contains three components, whereas for that above the transition only two components are visible and a fit with two Gaussian components yields only slightly too large values for the FWHM. In spite of that, this

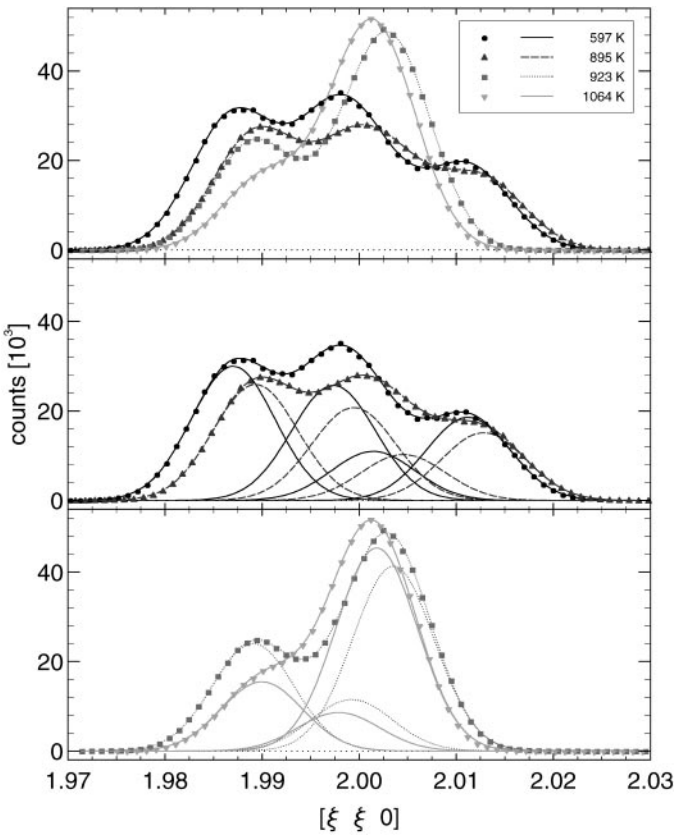

FIG. 10. Longitudinal scans of the 2 2 0 fluorite structure reflection of $CeO_{1.765}$ at 597 K, 895 K, 923 K, 1064 K. (Top) Comparison of the fit functions for all four temperatures. Each function consists of four (597 K and 895 K) or three (923 K and 1064 K) Gaussian components, respectively. (Middle) For each profile taken below the phase transition (597 K and 895 K) the four Gaussian components and the sum function are plotted. (Bottom) The same for the profiles taken above the phase transition (923 K and 1064 K, three components each). (Cf. Table 4.)

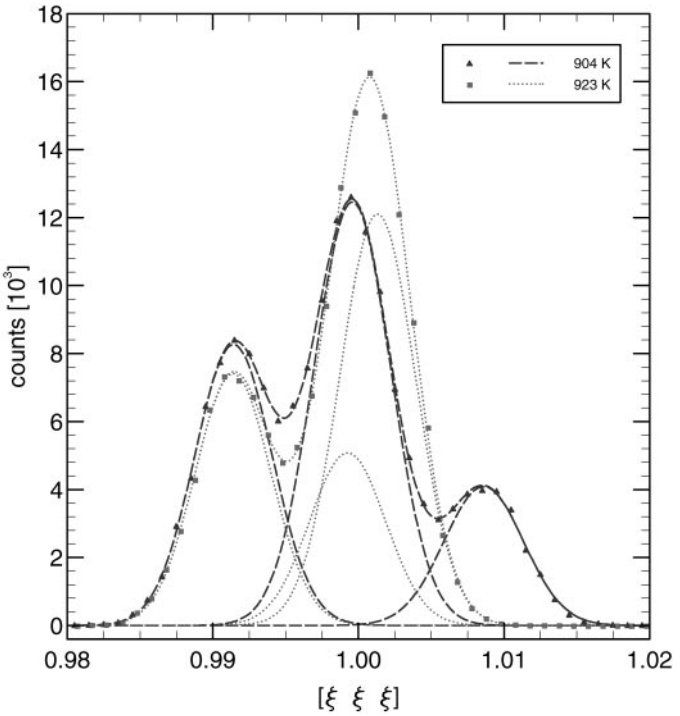

FIG. 11. Longitudinal scans of the 1 1 1 fluorite structure reflection of $CeO_{1.765}$ at 904 K and 923 K, i.e., below and above the phase transition. For each temperature the three Gaussian components and the sum function are plotted.

profile was finally fitted with three Gaussian components, too, for reasons explained later. The fit parameters are shown in Table 4.

DISCUSSION

The observations presented above will now be analyzed with respect to the CeO_y phase diagram. Figure 12 shows the location of the measurements taken for $CeO_{1.800}$ and $CeO_{1.765}$ (this work) as well as for $CeO_{1.698}$ (see (3, 4)) and the observed phase transitions, respectively, within the phase diagram by Ricken *et al.* (1). It will turn out that in contrast to the current phase diagram published by ASM International (2) that by Ricken *et al.* is suitable to explain our experimental results.

The Sample $CeO_{1.698}$

Here, the situation is rather simple. The structure determination by neutron diffraction proved that this sample (at least its dominant volume fraction) consists of the phase Ce_7O_{12} (3, 4). The phase transition found at 1072 K can be undoubtedly identified with that at 1084 K in the phase diagram by Ricken. At that transition the rhombohedral low-temperature phase Ce_7O_{12} vanishes (3, 4). It is not stable up to 1300 K, as assumed by Bevan and Kordis (5). Above that transition no superstructure reflections could be found (3, 4), so it can be assumed that there is no long-range order of the oxygen vacancies.

The Sample $CeO_{1.765}$

The diffraction patterns taken at the DNS already showed that this sample contains considerable volume fractions of Ce_7O_{12} as well as of a second phase. The measurements at the UNIDAS showed that the superstructure reflections not belonging to Ce_7O_{12} vanish at 911 K. Below that phase transition the 2 2 0 fluorite structure reflection is split longitudinally into four and above it into three components. The 0 0 4 fluorite structure reflection is split into two components, below as well as above the transition, where the distance between the two components is small above the transition and becomes smaller with increasing temperature. (See Table 4.)

It is easy to understand the observed reflection splitting within the framework of the phase diagram by Ricken *et al.* Below the phase transition the splitting of the 0 0 4 is caused by the coexistence of two rhombohedral phases, Ce_7O_{12} and the phase at $y \approx 1.79$ labeled p_2 in the phase diagram. The distance $\Delta|\mathbf{Q}|$ between the two reflection components at 598 K yields a relative difference $\Delta a/a \approx \Delta|\mathbf{Q}|/|\mathbf{Q}| = 0.0055(1)$ for the pseudocubic lattice parameter. Using the relationship $\Delta a/\Delta y = -0.40$ Å (6) the difference between the two compositions is determined as $\Delta y = 0.076(2)$. Considering the homogeneity range of Ce_7O_{12} (3, 4), it is appropriate to assume a composition of $y = 1.720$ (at the border of the homogeneity range) for that component. With that, the composition $y = 1.796$ is derived for the other component p_2.

For the 2 2 0 reflection, there is an additional splitting caused by different orientations of the twin domains for both rhombohedral phases. In the case of Ce_7O_{12}, that reflection is a superposition of rhombohedral reflections of the types $\bar{3}\,2\,1_r$ and $3\,1\,0_r$. Because each rhombohedral phase contributes two components, the 2 2 0 is split four-fold.

For Ce_7O_{12} with a rhombohedral angle $\alpha = 99.42^\circ$ (3, 4) the relative difference in the length of the two reciprocal vectors $\bar{3}\,2\,1_r$ and $3\,1\,0_r$ is $\Delta|\mathbf{Q}|/|\mathbf{Q}| = 0.0038$. At 597 K the relative difference in the reciprocal vector length between neighboring components of the 2 2 0 reflection are 0.0052(3), 0.0020(6), and 0.0049(4), respectively (see Table 4). It is true that none of these values matches the expected value for Ce_7O_{12} very well, but considering the changes observed at the phase transition, it is evident that the first and the second components belong to Ce_7O_{12} and the third and the fourth components belong to the phase p_2. According to the reflection splittings caused by the orientation domains ($\Delta|\mathbf{Q}|/|\mathbf{Q}| = 0.0052$ for Ce_7O_{12} and 0.0049 for p_2), the rhombohedral distortion seems to be roughly equal for the two phases.

TABLE 4

Parameters of the Profile Fits for the Longitudinal Scans of the 0 0 4, 2 2 0, and 1 1 1 Reflections for $CeO_{1.765}$ Using the Function $\sum_i A_i \exp(-(\xi - B_i)^2/2\sigma_i^2)$ The FWHM Values of the Gaussian Components are $w_i = \sigma_i \sqrt{8 \ln 2}\, f(2\pi/a)$, where the Geometric Factor f is 1, $\sqrt{2}$, and $\sqrt{3}$ for 0 0 4, 2 2 0, and 1 1 1, Respectively. I is the Integral and S the Center of Gravity of the Fit Function

Range	T (K)	I	S	i	$A_i(10^2)$	B_i	σ_i	w_i (Å^{-1})
					0 0 4 Reflection			
R1	598	168.5	3.9991	1	39.0(4)	3.9890(2)	0.0094(2)	0.0251(1)
				2	31.2(3)	4.0110(3)	0.0099(2)	0.0265(1)
R1	680	156.4	3.9998	1	35.8(4)	3.9896(2)	0.0093(2)	0.0248(1)
				2	29.4(3)	4.0115(3)	0.0099(2)	0.0264(1)
R1	760	136.6	4.0009	1	31.1(5)	3.9906(2)	0.0091(2)	0.0243(1)
				2	26.0(4)	4.0122(3)	0.0100(2)	0.0267(1)
R1	840	130.0	4.0015	1	31.1(4)	3.9917(2)	0.0091(1)	0.0242(1)
				2	23.9(3)	4.0132(3)	0.0098(2)	0.0261(1)
R1	895	124.6	4.0011	1	32.1(6)	3.9928(3)	0.0093(2)	0.0248(1)
				2	19.9(5)	4.0134(5)	0.0100(3)	0.0266(1)
R2	923	151.6	3.9997	1	38.1(4)	3.9932(1)	0.0093(1)	0.0248(1)
				2	26.7(5)	4.0090(2)	0.0093(1)	0.0248(1)
R2	1064	173.2	4.0000	1	37(2)	3.9947(3)	0.0093(1)	0.0248(1)
				2	37(2)	4.0052(3)	0.0093(1)	0.0248(1)
					2 2 0 Reflection			
R1	597	921.6	1.9973	1	30(0)	1.9870(1)	0.00431(3)	0.0163(1)
				2	25(3)	1.9973(4)	0.00431(3)	0.0163(1)
				3	10(3)	2.0014(7)	0.00431(3)	0.0163(1)
				4	18(1)	2.0112(1)	0.00431(3)	0.0163(1)
R1	757	897.1	1.9980	1	29(0)	1.9880(1)	0.00434(2)	0.0164(1)
				2	22(3)	1.9982(3)	0.00434(2)	0.0164(1)
				3	14(3)	2.0018(5)	0.00434(2)	0.0164(1)
				4	18(1)	2.0118(1)	0.00434(2)	0.0164(1)
R1	895	783.7	1.9993	1	26(0)	1.9893(1)	0.00434(2)	0.0163(1)
				2	20(1)	1.9994(2)	0.00434(2)	0.0163(1)
				3	10(1)	2.0045(4)	0.00434(2)	0.0163(1)
				4	15(1)	2.0128(1)	0.00434(2)	0.0163(1)
R2	923	806.9	1.9984	1	24(0)	1.9891(1)	0.00419(3)	0.0158(1)
				2	11(2)	1.9992(3)	0.00419(3)	0.0158(1)
				3	41(2)	2.0035(1)	0.00419(3)	0.0158(1)
R2	1064	729.6	1.9987	1	15(1)	1.9900(1)	0.00419(3)	0.0158(1)
				2	9(2)	1.9979(8)	0.00419(3)	0.0158(1)
				3	45(3)	2.0018(1)	0.00419(3)	0.0158(1)
					1 1 1 Reflection			
R1	904	165.4	0.9984	1	8.3(1)	0.9914(1)	0.00265(4)	0.0122(2)
				2	12.5(1)	0.9996(1)	0.00264(3)	0.0122(2)
				3	4.1(1)	1.0086(1)	0.00273(6)	0.0126(3)
R2	923	160.6	0.9979	1	7.4(1)	0.9914(1)	0.00261(4)	0.0120(2)
				2	5(2)	0.9993(4)	0.00261(4)	0.0120(2)
				3	12(2)	1.0013(2)	0.00261(4)	0.0120(2)

Calculating the mean reflection positions of the components belonging to each phase yields 1.9922(3) for Ce_7O_{12} and 2.0063(4) for p_2. The relative difference between these vector lengths $\Delta|\mathbf{Q}|/|\mathbf{Q}| = 0.0071(4)$, that is due to the different compositions of the two phases, is considerably larger than the value 0.0055 determined for the 0 0 4 reflection, so the composition of p_2 derived above may be rather approximate.

Above the phase transition, the components belonging to Ce_7O_{12} persist and, as a second phase, the cubic α' structure is present now. When the temperature is increased, the oxygen content comes closer to that of Ce_7O_{12}, as can be seen in the phase diagram. Corresponding to that, the distance between the two components of the 0 0 4 reflection decreases. For the 2 2 0 reflection, the contribution of the cubic α' phase consists of only one component, so that the reflection is split three-fold above the phase transition.

According to that interpretation, the 1 1 1 reflection should be split into four components below and into three components above the transition (containing the Ce_7O_{12}

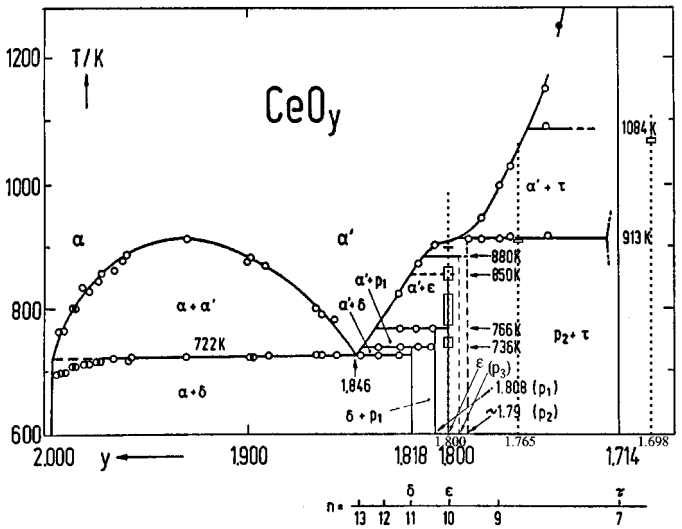

FIG. 12. Comparison of the results from the neutron diffraction measurements on $CeO_{1.800}$, $CeO_{1.765}$ (this work), and $CeO_{1.698}$ (3, 4) (black) with the CeO_y phase diagram of Ricken *et al.* (1, 10) determined from specific heat measurements (gray). (The phase p_3 is added according to Figure 6.18 in (10).) The dotted black lines ($\cdots$) show the temperature range of the measurements for each sample. The rectangles mark the observed phase transitions where the upper boundary gives the transition temperature when the temperature is raised and the lower boundary when it is lowered, so the height of the rectangles shows the hysteresis of the transition. The temperatures given in the phase diagram were measured when the temperature was raised, so the upper boundaries of the rectangles have to be compared with the phase transition temperatures in the diagram.

reflections of the types $\bar{1}\,2\,0_r$ and $1\,1\,1_r$). Although there is experimental evidence for only three components below and two components above the phase transition, it may be assumed that below the transition, the peak in the middle that has the highest intensity consists of two components, that cannot be separated within the experimental resolution. Above the transition, the profile can be fit with three components, as shown in Fig. 11.

The partial intensities of the fluorite structure reflection components as well as the intensity of the Ce_7O_{12} reflection $\bar{1}\,3\,0_r$ at 1064 K indicate that there is still a large volume fraction of Ce_7O_{12} present, in quantitative contradiction to the phase diagram. According to our measurements, the border of the α' phase should be located at larger y values than those given in the phase diagram by Ricken (see Fig. 12).

The Sample $CeO_{1.800}$

Here, the situation is most complicated. All the phase transitions observed at the UNIDAS when raising the temperature, i.e., the upper boundaries of the rectangles, can be identified with the transitions shown in the phase diagram. However, the temperature values in the phase diagram have to be shifted downwards by up to 27 K. These shifts do not mean any significant discrepancy because the specimens and particularly the experimental facilities as well as the experimental procedures (e.g., the higher heating rates in the specific heat measurements) were quite different.

The fact that the phase transition with the lowest transition temperature could be observed indicates that the actual oxygen content of the sample is slightly higher than that determined from the pseudocubic lattice parameter, i.e., $y \approx 1.801$.

In the ranges R1–R3 the 2 2 0 reflection is split into two components. The distance between these components approximately matches the splitting magnitude for Ce_7O_{12} caused by the different orientations of the twin domains. In the range R4 this is true for the first two components of the three-fold splitting of the 2 2 0 reflection. Consequently, it may be assumed that all the phases occurring in the ranges R1–R3 have a rhombohedral structure with a lattice distortion comparable to that of Ce_7O_{12}. This also matches the fact that the 0 0 4 is not split in R1.

As for $CeO_{1.800}$ there could not be detected any additional splitting in the ranges R1–R4 caused by different compositions, it has to be assumed that the oxygen contents of all the occurring phases differ only slightly, in obvious agreement with the phase diagram. In the range R4, in addition to a phase with ordered oxygen vacancies and a rhombohedral superstructure, there occurs the phase α' which has a significantly higher oxygen content. This phase causes the third component of the 2 2 0 reflection (see Table 3). (Unfortunately, the profile of the 0 0 4 reflection was only measured in the ranges R1 and R5 but not in R4!).

Ricken assumed that the composition of the phase p_3 is approximately $CeO_{1.793}$ (10). But from the fact that the α' phase could not be found in the range R3, it follows that the oxygen content of that phase must be much closer to the mean oxygen content of the sample crystal, i.e., only slightly lower than the oxygen content $y = 1.800$ of the neighboring phase ε. Otherwise, if its oxygen content were as low as assumed by Ricken, the volume fraction of the coexisting α' phase had to be high enough to be detected.

Now we turn to the discussion of the observed superstructure reflections (Fig. 4). At the first phase transition T1, two very weak reflections at $\xi\xi\xi/2$, $\xi = 1.47$ and 1.755 disappear, confirming that a small volume fraction of the phase p_1, that existed in the range R1, vanishes here. The major volume fraction in the sample belongs to the phase ε, in R1 as well as in R2. In each of the ranges R2–R4, there exists only a single phase with a superstructure; there are the phases ε in the range R2, p_3 in R3, and p_2 in R4.

It might be expected that the superstructure reflection pattern would completely change at each of the phase transitions T2–T4. However, the reflection $\xi\xi\xi/2$, $\xi = 1.84$ varies only slightly in its intensity. As well, the shift of the reflection $\xi\xi 2 - \xi/2$, $\xi = 1.845$ at the transition T2 is only

very small. However, this is not in contradiction to our interpretation; it only indicates that all these phases are structurally closely related to each other.

In summary, the neutron diffraction investigations showed that the phase diagram by Ricken *et al.* is qualitatively correct for the composition range $1.8 \geq y \geq 1.7$. Only the precise oxygen contents of the phases in that composition range and the precise phase transition temperatures are questionable. Moreover, the diffraction measurements indicate that the structures of all the phases p_1, ε, p_3, and p_2 are of rhombohedral symmetry.

ACKNOWLEDGMENTS

We thank G. Eckold for his support on the specimen preparation and for the helpful discussions. We also thank W. Aßmus for the CeO_2 single-crystal growth.

REFERENCES

1. M. Ricken, J. Nölting, and I. Riess, *J.Solid State Chem.* **54,** 89 (1984).
2. "Binary Alloy Phase Diagrams" (Th. B. Massalski, H. Okamoto, P. R. Subramanian, and L. Kacprzak, Eds.), *Second Edition*, Vol. 2. ASM International, Materials Park, OH, 1990, 1992.
3. E. A. Kümmerle and G. Heger, *J. Solid State Chem.* **147,** 485 (1999).
4. E. Kümmerle, Doctoral Thesis, Forschungszentrum Jülich Report No. Jül-3576, 1998.
5. D. J. M. Bevan and J. Kordis, *J. Inorg. Nucl. Chem.* **26,** 1509 (1964).
6. S. P. Ray, A. S. Nowick, and D. E. Cox, *J. Solid State Chem.* **15,** 344 (1975).
7. B. Touzelin, *J. Nucl. Mater.* **101,** 92 (1981).
8. J. R. Sims and R. N. Blumenthal, *High Temp. Sci.* **8,** 99 (1976).
9. H.-W. Chiang, R. N. Blumenthal, and R. A. Fournelle, *Solid State Ionics* **66,** 85 (1993).
10. M. Ricken, *Thermodynamische Untersuchungen am System* CeO_2–$CeO_{1.714}$, Doctoral Thesis, University of Göttingen, 1983.